

FEATURE ARTICLE

Microgel Colloidal Crystals

L. Andrew Lyon,* Justin D. Debord, Saet Byul Debord, Clinton D. Jones,
Jonathan G. McGrath, and Michael J. Serpe

School of Chemistry and Biochemistry, Georgia Institute of Technology, Atlanta, Georgia 30332-0400

Received: April 6, 2004; In Final Form: May 26, 2004

Colloidal crystals assembled from stimuli-sensitive hydrogel particles composed largely of the thermoresponsive polymer poly(*N*-isopropylacrylamide) display unusual phase behavior because of the inherent “softness” of their interaction potentials as well as the particle thermoresponsivity. In this contribution, we review results from our group that illustrate the use of such soft-sphere building blocks in the construction of colloidal crystals. First, we describe the utility of temperature-induced volume phase transitions in controlling the crystallization and melting of the colloidal crystals. These methods then enable the study of the complex phase behavior of certain types of microgels. For example, it is proposed that multiple weak attractive interactions between particles can drive crystallization at particle concentrations well below the hard-sphere freezing point. Finally, the utility of soft-sphere crystals in the development of new photonic materials is presented in examples of laser direct writing and photopatterning of colloidal crystals based on a photothermally directed crystallization method.

Introduction

While colloidal crystalline assemblies have been a focus of scientific curiosity for less than 50 years,^{1,2} natural colloidal assemblies such as gemstone opals^{3,4} have fascinated man since before recorded history. Then as now, interest in such materials is strongly connected to the brilliant optical properties that evolve as the refractive index periodicity approaches the wavelength of visible light.⁵ In more recent times, investigators have initiated efforts aimed at understanding the fundamental details of such structures, along with the mechanisms by which they form in nature and the laboratory. Much of that field has benefited from the advent of optical and electron microscopy techniques that allow for direct observation of the 3D structure of these materials^{3–15} and, more recently, the dynamics of colloidal media in different regions of phase space.^{16–19} Studies such as these have, in turn, fed the curiosity of those pursuing materials displaying truly unique and powerful optical effects such as omnidirectional photonic band gaps (OPBG)^{20–27} or superprismatic refraction.^{28–33} Thus, the broad interest in the optics of periodic colloidal assemblies has come full circle; the mesmerizing beauty of diffraction continues to hold our collective attention from prehistory to the intense scientific environment of modern times.

Our group's interest is also in part aimed at exploring the optical properties of colloidal assemblies.^{34,35} However, the scientific focus is mainly on the side of the particles of which the assemblies are composed.^{36–38} In this article, we will review the group's recent efforts in understanding the assembly of soft, thermoresponsive, hydrogel particles into three-dimensionally ordered crystals. Initially, an overview of the fundamental

properties of these primitive colloidal assemblies will be presented. The ability to access high volume fraction crystals from thermoresponsive particles will be discussed, as well as investigations into the fundamental phase behavior of such particles. We will then review our efforts in the laser-based patterning of colloidal crystals via photothermal effects.

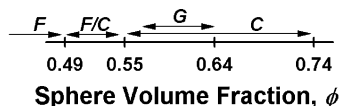
Colloidal Crystals: Assembly and Optical Properties

It is proposed that the formation of gemstone opals took place through the steps of silica dissolution, precipitation (as monodisperse spherical particles), slow sedimentation or filtration into a close-packed arrangement, and finally infiltration with and sintering of differentially hydrated silica.^{6,7,13,39} The phase diagram governing the behavior of spherical, mutually repulsive colloids in a fluid predicts that the lowest-energy conformation of such a close-packed system is the face-centered cubic (fcc) structure,^{40,41} which, as conjectured by Kepler in 1611,⁴² has a particle fill fraction of 74%. This value has been confirmed in both macroscale and microscale model systems and has also been the recent subject of mathematical proof.^{41,43–46}

To form ordered assemblies from monodisperse spheres prepared in the laboratory, researchers have traditionally mimicked the proposed natural process, relying on slow sedimentation,^{39,47,48} gentle evaporation of solvent,⁴⁹ or filtration^{50,51} to force the colloidal particles into close contact. These methods all provide for assembly that is slow and gentle enough to allow the particles to pack into the thermodynamically preferred arrangement with low defect densities. Increasing the rate of packing typically increases the defect density due to kinetic trapping of particles in nonequilibrium conformations. Classical studies of colloidal phase behavior have provided more insight into the details of particle packing. In these experiments,

* To whom correspondence should be addressed. E-mail: lyon@chemistry.gatech.edu.

SCHEME 1: Representation of the Hard-Sphere Phase Diagram Showing the Fluid (F), Crystalline (C), Coexistence (F/C), and Glassy (G) Regions



monodisperse, noninteracting spheres were suspended in fluids over a range of particle volume fractions.^{39,40} Visual inspection of the systems then allowed for the determination of the phase present. At volume fractions below $\sim 49\%$, a disordered fluid is observed, where particle positions are not correlated over long distances. Between ~ 49 and $\sim 55\%$ sphere volume fraction, an ordered crystal phase (55% volume fraction) stands in equilibrium coexistence with the less dense fluid phase (49%). Above 55% volume fraction, the crystalline structure dominates, where particle motion and position are highly correlated over long distances. Under these experimental conditions, it is interesting that the densest close-packed arrangement (74% volume fraction) is never observed. Instead, with increasing particle concentration an increase in viscosity is observed, which is a macroscopic indicator of the increased interactions between particles and a concomitant decrease in the particle diffusion coefficient. This condition results in the formation of a glassy, jammed, or trapped phase, where the particles are forced into close contact without the free-volume-minimizing condition observed in long-range periodic structures.^{52–58} Of course, this phase does not display the brilliant opalescence of the ordered phases. A variety of predictions and measurements have been made to quantify the maximum volume fraction of “randomly” packed spheres, with the values ranging about that for a Bernal glass (64%).^{41,52,53,59} Together, these experiments, predictions, and mathematical models paint a picture of the colloidal phases that is represented in a simple form as Scheme 1.

The optical properties of simple colloidal crystals can be described using a formalism originally developed for X-ray diffraction in molecular crystals. Bragg’s law

$$m\lambda = 2nd \sin \theta \quad (1)$$

relates the diffracted wavelength (λ) and the diffraction order ($m = 1, 2, 3, \dots$) to the refractive index of the medium (n), the lattice spacing (d), and the angle of incidence relative to the lattice plane (θ). For colloidal particles of a known diameter, D , the lattice spacing can be calculated for any set of Miller indices h , k , and l .

$$d_{hkl} = \frac{1.414D}{(h^2 + k^2 + l^2)^{1/2}} \quad (2)$$

To a first approximation, this simple mathematical treatment is sufficient for systems wherein the refractive index of the assembly is accurately represented by a weighted sum of the refractive indices of the two phases. This is applicable for the low index contrast microgel crystals described below. We will therefore not concern ourselves here with more complex treatments required for modeling omnidirectional PBG or superprism effects.

Thermoresponsive Microgels

The building blocks used by our group for the assembly of colloidal crystals are most commonly thermoresponsive microgel particles.^{60–62} A few other groups have explored the assembly of soft building blocks as well.^{63–71} Characteristic of these

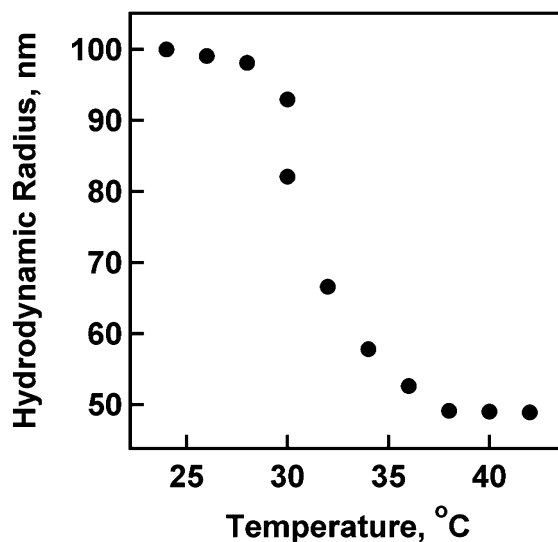


Figure 1. Typical phase-transition behavior as a function of temperature for pNIPAm microgels in water as measured by dynamic light scattering.

particles in aqueous media is the large magnitude volume phase transition they undergo in response to temperature. For the common polymer poly(*N*-isopropylacrylamide) (pNIPAm),⁷² this transition occurs at $\sim 31^\circ\text{C}$. Below this lower critical solution temperature (LCST), pNIPAm is well solvated in aqueous milieu, whereas above that temperature, an entropically driven hydrophobic collapse of the material is observed. High molecular weight pNIPAm homopolymer displays this behavior via a nearly first-order coil-to-globule transition.⁷³ Similarly, cross-linked macrogels or microgels undergo a reversible volume change due to the expulsion of solvent from the network.^{74–77} Fully swollen particles can contain up to 99% water by volume below the LCST, with collapsed microgels containing $\sim 20\%$ or less water by volume. Figure 1 shows the size dependence of some typical pNIPAm microgels in aqueous solution as a function of temperature. The position, magnitude, and breadth of the volume phase transition (VPT) can be manipulated with the addition of comonomers,⁷⁸ cross-linker identity and concentration,⁷⁹ and also by changes to the surrounding medium.⁸⁰ The use of these polymers in the assembly of colloidal crystals was first motivated by goals of tunable or switchable optical materials, as has been described previously for other assemblies.^{32,65,81–86} As described below, the utility of such building blocks extends beyond those initial goals by enabling the fabrication of a range of previously unattainable materials.

Synthesis. Microgels are synthesized by free-radical precipitation polymerization in aqueous solution.^{60–62} Ammonium persulfate (APS) is thermally decomposed at 70°C to initiate the polymerization of NIPAm, *N,N'*-methylenebisacrylamide (cross linker), and various other functional co-monomers such as acrylic acid (AAc) in the presence of the surfactant sodium dodecyl sulfate (SDS). In these syntheses, the initial solution is homogeneous, with the SDS concentration (0 to 1 mM) lying far below the critical micelle concentration (CMC at $25^\circ\text{C} \approx 8\text{ mM}$) and all monomers being fully water-soluble. However, once polymerization is initiated, the propagating polymer chains rapidly reach a critical chain length for phase separation from the solvent. This coil-to-globule phase transition acts to form nuclei for further particle growth.^{62,73} A key aspect of this synthesis is the ability to form highly monodisperse particles that are appropriate for crystallization. The polydispersity, as determined by dynamic light scattering, typically lies below $\pm 14\%$. Note that dynamic light scattering is not a well-defined

method for determining polydispersity and that the dispersity is often overestimated. Nonetheless, we cannot precisely determine polydispersities by techniques such as electron microscopy because of particle deformation and dehydration. Regardless, we observe excellent crystallization for particles that are less than $\pm 14\%$ polydisperse by dynamic light scattering. The good monodispersity in these preparations is apparently facilitated by the inherently rapid initiation and propagation in the APS/NIPAm system, along with the propensity for oligoradicals to precipitate on preformed nuclei as opposed to the homonucleation of new particles. This temporally limits the formation of particles to very early stages of the reaction, with all further monomer consumption going toward the growth of those particles and not new particle nucleation. We have taken advantage of this effect to synthesize a wide range of core/shell-type microgels via a seeded precipitation polymerization method that is described in detail elsewhere.^{87–94} Particle size can be controlled through variation of the surfactant, initiator, and initial monomer concentrations.⁶⁰ The particle-size distribution is an important consideration for ordered systems and can also be minimized by taking preliminary cleaning/filtration steps before synthesis.⁹⁴

Experimental Results

Microgel Assembly. Of primary importance for the work described herein is that lightly cross-linked microgels composed of pNIPAm prepared by the synthetic methods described above possess the properties required for efficient entropic assembly. Colloidal dispersions with a high degree of particle monodispersity are easily accessible, thus providing for the homogeneous population of building blocks required for such a periodic assembly. It is expected that such particles will display a predominantly repulsive interaction potential due to mutual volume exclusion. Although the use of the persulfate initiator affords particles that have some anionic surface charge, the electrophoretic mobility of such particles is typically very modest, so electrostatic repulsion is likely not a dominant contributor to the pair potential. Furthermore, it is reasonable to expect that a highly solvent swollen polymer network will have an effective Hamaker constant that is quite small, making van der Waals attraction a minor contribution to particle interactions. Finally, below the polymer LCST, the material is extremely hydrophilic, which eliminates hydrophobic aggregation of the polymer spheres. Thus, pNIPAm microgels can be considered to have little to no attractive contribution to the overall interaction energy, along with a short-range repulsive force based on volume exclusion and chain elasticity.

Given the fact that these particles appear to have the appropriate physical properties for crystallization, we investigated the phase behavior following concentration into a close-packed arrangement.³⁵ Note that the traditional methods used for silica, polystyrene, or poly(methyl methacrylate) particle assembly cannot be used here. Hydrogel particles are too buoyant in water to sediment at an appreciable rate, and filtration or slow evaporation methods are inappropriate because of the extreme solvation of the particles themselves. Forced sedimentation by centrifugation was therefore employed to force the particles into close contact without drying. Centrifugation of an aqueous microgel dispersion ($\sim 16\,000\text{ g}$, 1 h) yields a weakly colored viscous pellet such as that shown in Figure 2(inset) for $\sim 280\text{-nm}$ -diameter pNIPAm-co-AAc particles.^{34,35} The accompanying extinction spectrum of the material shows no strong diffraction peak and therefore no obvious evidence of long-range ordering. The lack of macroscopic crystallites and the

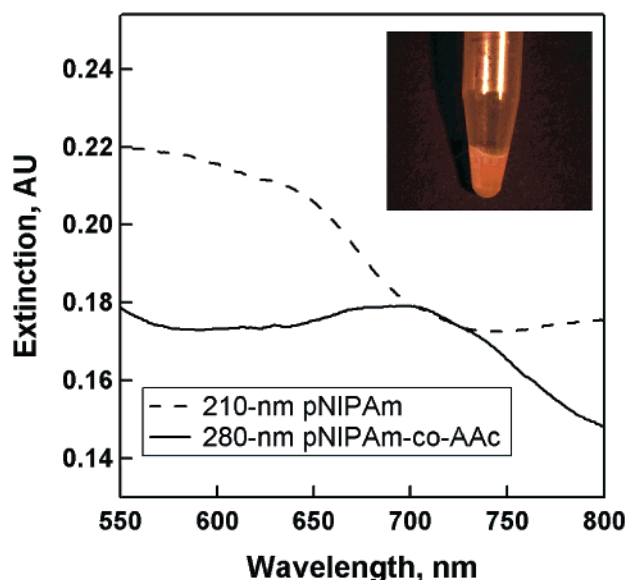


Figure 2. Extinction spectra of glassy materials prepared from 280-nm-diameter pNIPAm-co-AAc (10% AAc) particles (solid line) and 210-nm-diameter pNIPAm particles (dashed line). (Inset) Photograph of a centrifuged pellet of pNIPAm-co-AAc microgel particles.

high particle volume fraction are indicative of a disordered, glassy, or jammed phase. This is not surprising, given the rather rapid and harsh assembly method. It is unlikely that the system has assembled under conditions that favor the lowest-energy arrangement.

Unlike a traditional nonresponsive, hard-sphere system, close-packed assemblies of thermoresponsive particles allow for thermal tuning of the effective volume fraction.^{34,36} Although the sample depicted in Figure 2 is jammed in its current state, warming the material above the pNIPAm LCST causes particle deswelling. This effectively reduces the particle volume fraction, causing a jammed sample to become fluid because of larger interparticle distances. The particle translational diffusion coefficient increases, and upon cooling to room temperature, the sample spontaneously assembles into the thermodynamically preferred crystalline state. This can be seen in Figure 3, which depicts the three different states of the assembly during the annealing process. Figure 3 (bottom) shows the extinction spectra for two different samples following a single annealing cycle. Note that a sharp Bragg peak, which corresponds to first-order diffraction from the (111) face of the fcc crystal, is now present in each spectrum. The sharpness of the peak is indicative of the spectral homogeneity of the sample, as well as the relatively low refractive index contrast between the particles and the water that fills the interstitial voids.

When larger particles are used to form such assemblies, the order of the system can be observed directly by optical microscopy. Figure 4 illustrates the packing obtained following the annealing of a sample containing 810-nm-diameter pNIPAm-co-acrylic acid particles, as observed by differential interference contrast (DIC) microscopy. The fcc (111) face is ordered in the plane of the container wall, as is typical for the crystallization of colloidal particles. Laser scanning confocal microscopy of a similar array that has been fluorescently dyed illustrates the regular ABCA packing of the fcc structure (Figure 5).

Optical Tuning via Compression. The softness and thermoresponsivity of pNIPAm microgels allows for the facile tuning of the Bragg diffraction wavelength by simply altering the diameter of the microgels through deswelling.³⁴ In this

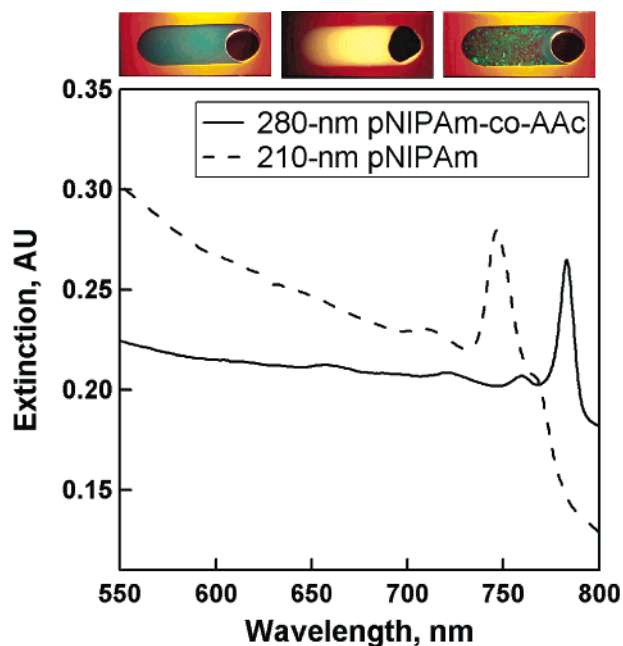


Figure 3. (Top) Photographs of pNIPAm microgel samples (~ 220 -nm-diameter particles) sandwiched between two glass coverslips separated by an elastomeric gasket. The three images show the sample in the disordered glassy or jammed state (left), the disordered fluid state (center), and the ordered crystalline state (right). (Bottom) Extinction spectra of the particle assemblies described in Figure 2 following thermal annealing to the crystalline state.

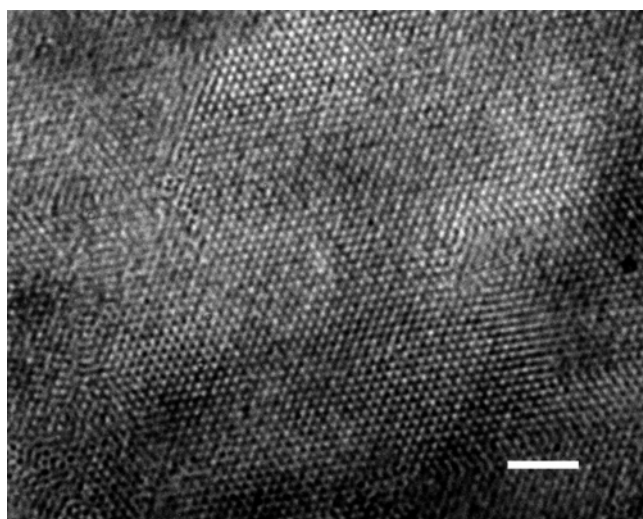


Figure 4. Differential interference contrast microscopy image of a microgel colloidal crystal assembled from ~ 810 -nm-diameter pNIPAm-co-AAc microgels. The scale bar is $10\ \mu\text{m}$.

process, a crystal is made via centrifugation and annealing, as described above. However, if centrifugation is performed at a temperature closer to the polymer LCST, then the particles are sedimented in a partially deswollen conformation. Removal of the supernatant water locks the particles into this higher-density phase, which must then lead to a smaller lattice constant. Because the particles are still quite solvated under these conditions, the samples can be thermally annealed to allow the jammed to crystalline phase transition. Because microgels prepared by precipitation polymerization display a continuous (non-first-order) volume phase transition (VPT) over the temperature range of ~ 29 – $33\ ^\circ\text{C}$,^{34,95} it is possible to approximately select the size of the microgels in the final assembly by selecting the temperature at which centrifugation is performed. This size

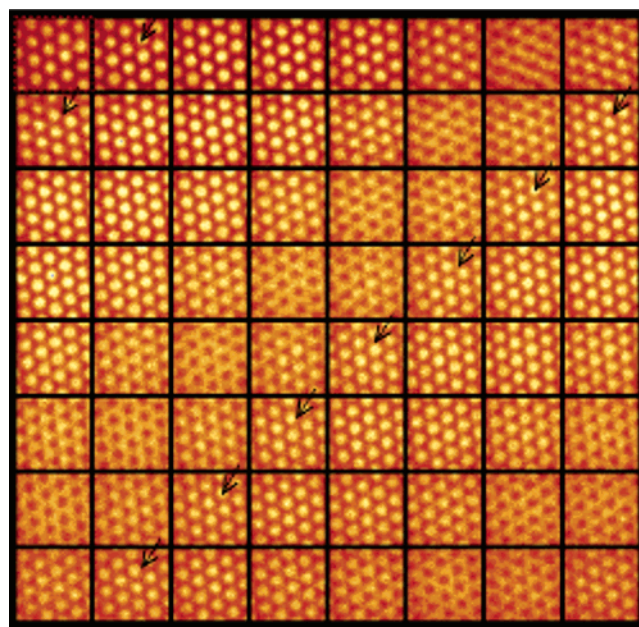


Figure 5. Series of optical sections obtained by laser scanning confocal microscopy of a fluorescein-dyed pNIPAm-co-AAc microgel colloidal crystal. Arrows are placed at the exact same location in each image to illustrate the ABCA packing in the crystal. The image size is $3.1 \times 3.1 \times 7.7\ \mu\text{m}^3$. Thus, the change in the z dimension between images is $\sim 0.12\ \mu\text{m}$.

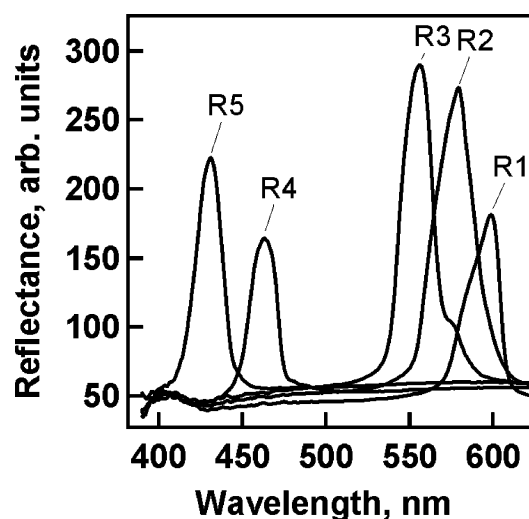


Figure 6. Reflectance spectra of wavelength-tuned pNIPAm colloidal crystal samples. Samples R1–R3 were centrifuged at $32\ ^\circ\text{C}$, and samples R4 and R5 were centrifuged at $35\ ^\circ\text{C}$. Centrifugation was then followed by removal of the supernatant solution. Reproduced with permission from *Adv. Mater.* **2002**, *14*, 658–661. Copyright 2002 Wiley-VCH.

selection allows for the theoretical determination of many different Bragg diffraction wavelengths from a single batch of particles. The results of representative experiments of this type are shown in Figure 6. As can be seen from the Figure, it is possible to tune the diffraction wavelength over almost 200 nm by controlling the size of these particular microgels, which is controlled by the temperature at which the microgels are centrifuged. In this case, the dilute solution particle diameter as determined by dynamic light scattering (DLS) was 260 nm. Table 1 shows the results of calculations of the crystal lattice spacing and particle size using eqs 1 and 2.

Microgel Crystal Phase Behavior. In an extension of the work described above, particle crystallization as a function of

TABLE 1: Calculated Interlayer (d) and Interparticle (a) Distances

sample	λ_{\max}	d (nm)	a (nm)
R1	600	225	275
R2	580	217	266
R3	555	208	254
R4	460	172	210
R5	430	161	197

volume fraction was observed directly by DIC microscopy.³⁶ Figure 7 shows a series of images taken of pNIPAm microgel colloidal crystals at various polymer concentrations. The effective volume fraction of the microgel crystals (ϕ_{eff}) was calculated on the basis of previous work done by Senff and Richtering.^{68,79} As discussed above, a colloidal dispersion is in the crystalline phase and fluid phase at ϕ_{eff} values above 0.545 and below 0.494, respectively; between these values, the system has a coexisting mixed phase composed of both fluid and crystal. This behavior is clearly seen in Figure 7. Panel a shows an “overpacked” sample prepared from pNIPAm at $\phi_{\text{eff}} = 1.96$, where ϕ_{eff} is based on the dilute solution particle size measured by DLS. Thus, values of $\phi_{\text{eff}} > 0.74$ indicate overpacking and particle deswelling, which was illustrated in Figure 6 by measurement of the stop band energies. Figure 7 shows further that as ϕ_{eff} is decreased by reducing the polymer concentration the lattice constant increases (panels b and c) and the crystal eventually melts (panel d) into a fluid phase at $\phi_{\text{eff}} = 0.49$, as predicted by the hard-sphere phase diagram.

In a related study, crystals were prepared from AAc microgel copolymers of pNIPAm (pNIPAm-co-AAc) with different particle concentrations.³⁶ The pH of the samples was held constant at ~ 3.8 so that $\sim 75\%$ of the AAc groups in the polymer network are protonated. Also, the ionic strength of the crystals was kept at ~ 1 mM, where the Debye–Hückel screening length is short compared to particle size, thus removing electrostatic repulsion as a significant contributor to crystallization. Panels a–g of Figure 8 show DIC images of pNIPAm-co-AAc crystals as a function of concentration. At $\phi_{\text{eff}} = 1.10$ (Figure 8a), the colloidal crystal is again overpacked because of the softness of the microgels. As with the experiments shown in Figure 7, further decreases in the polymer concentration lead to an expansion of the lattice (b–h) and the eventual melting of the crystal (i). However, the values of ϕ_{eff} for these samples suggest that the phase behavior is not at all hard-sphere-like because the observed melting point ($\phi_{\text{eff}} = 0.11$) is far below that which is predicted by the hard-sphere model (~ 0.49). Indeed, excellent crystallization is observed down to a ϕ_{eff} as low as 0.12 as shown in Figure 8h. Crystalline phases have been observed below the hard-sphere freezing point in highly charged microgel systems, where long-range attractive forces resulted in the coexistence of fluid and crystalline phases at low particle concentrations.^{17,96} Because the system presented in Figure 8 should not be strongly influenced by Coulombic forces (because of the short screening length), it is unlikely that the phase behavior we observe arises from such long-range attractive forces. Another interesting observation is that the particle size becomes larger as particle concentration decreases. In fact, the center-to-center distance (which may approximate the particle size in close-packed or nearly close-packed systems) is $1.5 \mu\text{m}$ in Figure 8h, which is ~ 1.8 times larger than the hydrodynamic radius measured in highly dilute solutions. This result suggests that at low particle concentrations the particles swell so that the particle volume fraction of the sample exceeds the hard-sphere freezing point. Because there is no obvious entropic driving force for particle crystallization at such low values of ϕ_{eff} , an attractive enthalpic

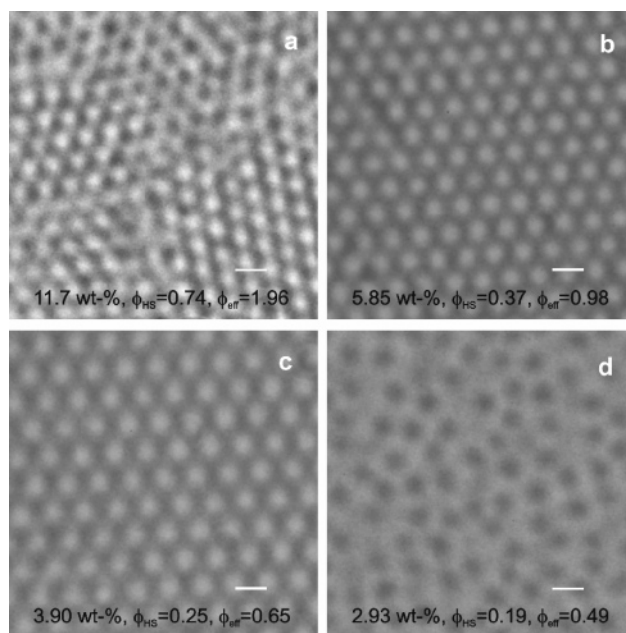


Figure 7. Differential interference contrast microscopy images of colloidal crystals assembled from pNIPAm microgel particles ($R_h = 380$ nm). The polymer concentrations in weight percent are indicated on each image, along with the hard-sphere (ϕ_{HS}) and effective (ϕ_{eff}) particle volume fractions. See the text for details concerning these values. Scale bars = $1 \mu\text{m}$. Reproduced with permission from *J. Phys. Chem. B* **2003**, 107, 2927–2932. Copyright 2003 American Chemical Society.

force may play a role in crystallization. Also, weak multibody interactions between particles could be involved in crystallization at such low particle concentrations. Although we have not conclusively determined the nature of these forces at the present time, we have hypothesized that the chemical composition of the microgels suggests the origin of the attractive forces.³⁶ Specifically, numerous acid/amide or acid/acid hydrogen-bonding interactions at the loosely cross-linked (hairy) surface of the microgels^{97,98} may be sufficient for the stabilization of crystals at these low effective volume fractions. Indirect evidence of this comes from the presence of “normal” phase behavior for pNIPAm (AAc-free) dispersions, as discussed above.³⁶ Regardless of the origin of the effect, these results illustrate the profound impact that soft-sphere building blocks can have on the phase behavior of colloidal media.

Composite Assemblies. In the above examples, we have used the temperature-induced volume phase transition of the particles to either anneal defects from the assembly or convert a glassy or jammed phase to a diffractive, crystalline material. These transitions were accomplished by simply warming the entire sample above the transition temperature and then cooling at a rate that allowed for recrystallization. It was also discovered in these studies that rapid cooling from the fluid state results in the formation of the kinetically trapped, nonphotonic glass. Thus, a simple temperature switch provides a method for reversible conversion between the photonic and nonphotonic state. Given the current interest in the patterning of self-assembled photonic materials, we reasoned that *localized or spatially controlled* heating via irradiation of a sample might provide a route to photolithography or laser direct writing of photonic assemblies. The goal was then to develop a method for photothermally exciting the assemblies via laser irradiation.

A convenient solution to this problem involves the co-assembly of colloidal Au particles with the responsive microgels.^{37,38} Excitation of the colloidal Au plasmon absorption

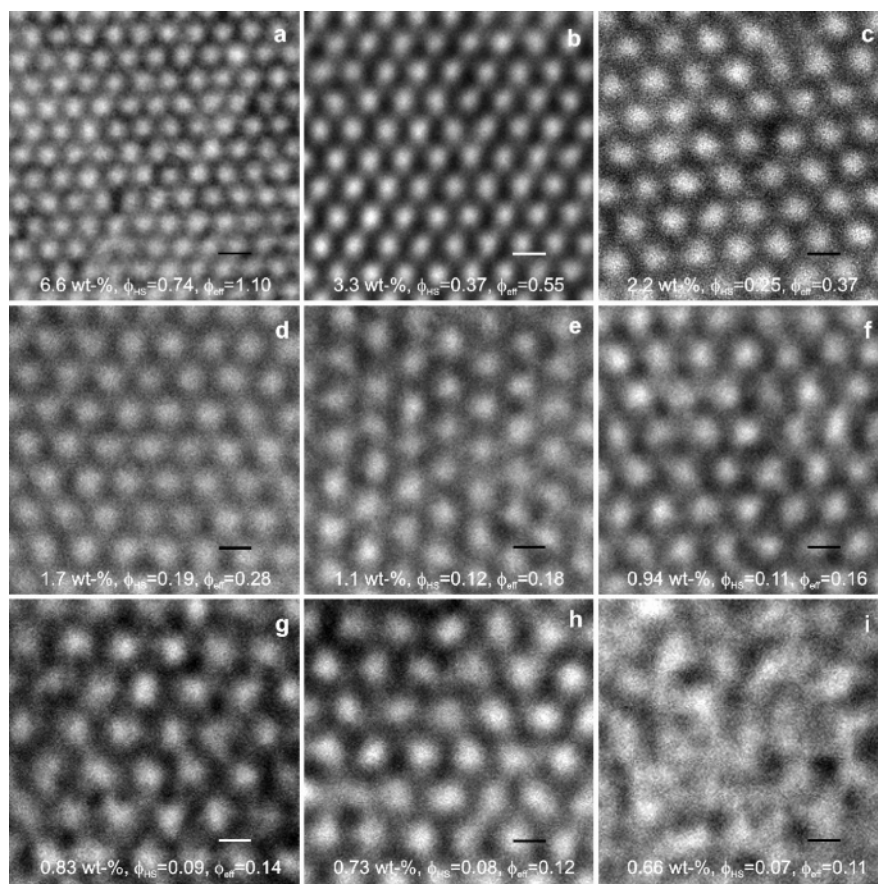
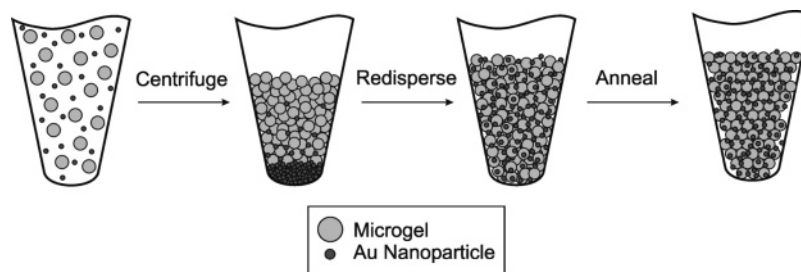


Figure 8. Differential interference contrast microscopy images of colloidal crystals assembled from pNIPAm-co-AAc microgel particles ($R_h = 410$ nm). The polymer concentrations in weight percent are indicated on each image, along with the hard-sphere (ϕ_{HS}) and effective (ϕ_{eff}) particle volume fractions. See the text for details concerning these values. Scale bars = $1\ \mu\text{m}$. Reproduced with permission from *J. Phys. Chem. B* **2003**, *107*, 2927–2932. Copyright 2003 American Chemical Society.

SCHEME 2: Assembly Process for Colloidal Au-Doped Microgel Colloidal Crystals^a



^a Reproduced with Permission from *J. Am. Chem. Soc.* **2003**, *125*, 460–465. Copyright 2003 American Chemical Society.

with a frequency-doubled Nd:YAG laser ($\lambda = 532$ nm) results in efficient local heating of the sample through nonradiative relaxation of the optically excited colloidal Au. This process relies on the large extinction coefficient of Au nanoparticles at the plasmon resonance ($\sim 1 \times 10^9\ \text{M}^{-1}\ \text{cm}^{-1}$ at 520 nm for 20-nm-diameter colloidal Au) and the extremely small photoemission quantum yield for such particles.⁹⁹ As a result, the energy absorbed upon plasmon excitation is largely re-emitted via nonradiative pathways, thereby heating the local environment surrounding the particle. The local heating provided by this fast nonradiative relaxation allows for the optically directed conversion of either jammed phases to crystalline assemblies or vice versa, depending on the illumination power and time.^{37,38}

Co-assembly of colloidal Au with the colloidal pNIPAm particles is accomplished by simply adding an aqueous colloidal Au suspension (16-nm diameter, citrate-stabilized) to the

microgel suspension prior to centrifugation.^{37,38} During the subsequent centrifugation step, the two types of particles sediment at different rates, with the smaller, denser colloidal Au separating from the solution faster than the larger but more buoyant microgel particles. Under these conditions, the Au particles do not noticeably aggregate and can be easily redispersed into the microgel mass (following decantation of the supernatant solution) by gentle sonication and agitation. This process is illustrated pictorially in Scheme 2.

Localized photothermal crystallization can be demonstrated by placing a sample cell consisting of a glassy or jammed-phase material in front of the Nd:YAG laser source. The nature of the resultant crystalline region can be controlled by the manipulation of various parameters such as laser power, Au colloid concentration, and ambient temperature. Figure 9 is a bright-field reflectance optical micrograph illustrating the results of irradiating a microgel/Au composite glassy material containing

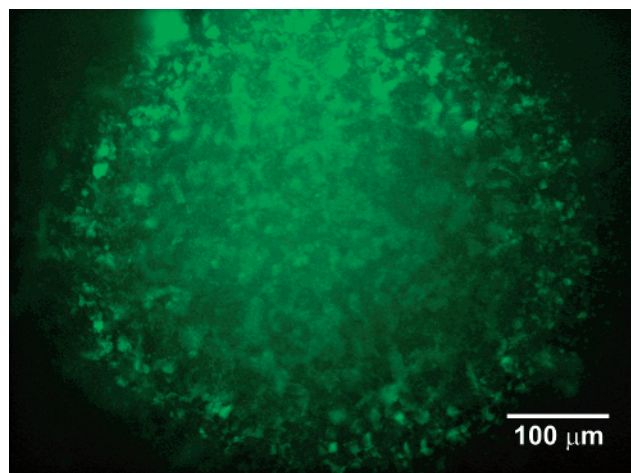


Figure 9. Optical micrograph of a crystalline region that has been photothermally introduced into a glassy sample containing 7.3×10^{13} Au particles/mL after 5 min of illumination. Reproduced with permission from *J. Am. Chem. Soc.* **2003**, 125, 460–465. Copyright 2003 American Chemical Society.

7.3×10^{13} Au particles/mL for 5 min with a 0.95-mm-diameter beam (incident power = 0.87 W/cm^2). A ~ 0.55 -mm-diameter circular region of brightly reflective polycrystalline material is observable, surrounded by a faintly colored region corresponding to the bulk glassy material. In contrast, samples that do not contain colloidal Au do not show any morphological changes upon illumination. These data are interpreted as being the result of photothermal heating, with the Au nanoparticles being the sensitizing moieties. Irradiation of the plasmon band results in local heating around the Au particles, thereby causing partial deswelling of the microgel particles. These particles are then able to diffuse more readily than in their swollen state, thus allowing for crystal nucleation and growth within the laser spot.

Microspectrophotometric interrogation^{37,38,100} of the photothermally patterned crystalline region clearly shows the dramatic change in optical properties relative to those of the original bulk glassy state. Figure 10b is the spectral image acquired from the indicated region of the real-space image (Figure 10a). The y axis of this image corresponds to the spatial dimension, and the x axis corresponds to wavelength. As such, the optical properties of a small portion of the crystalline region can be correlated directly with the image. Panels c–e of Figure 10 show representative line scans taken from different regions of the spectral image, thus illustrating the relative spectral homogeneity of the photothermally patterned crystalline region. These data are suggestive of relatively homogeneous crystal orientations and lattice constants. Conversely, the spectral image acquired from the bulk glassy material before irradiation shows no structure resulting from Bragg diffraction in the assembly.

Because excitation of the Au particles under certain conditions yields glass-to-crystal transitions, irradiation of precrystallized materials under higher-power conditions allows for the conversion of the crystalline material to a glassy one. The results of this process are shown in Figure 11, where now a circular glassy region is formed inside a brightly reflective bulk crystalline sample after only 22 s of laser irradiation at 3.4 W/cm^2 . In this case, the higher laser power induces a higher local temperature relative to ambient, thus producing a faster overall cooling rate, which acts to trap the sample in a jammed phase following cooling. These simple demonstrations illustrate the potential utility of photothermal manipulation of composite hydrogel assemblies.

Whereas the above examples take advantage of temperature differences between the irradiated regions and the ambient temperature to control the cooling rate and therefore the resultant phase, one can also imagine using spatial variations in flux

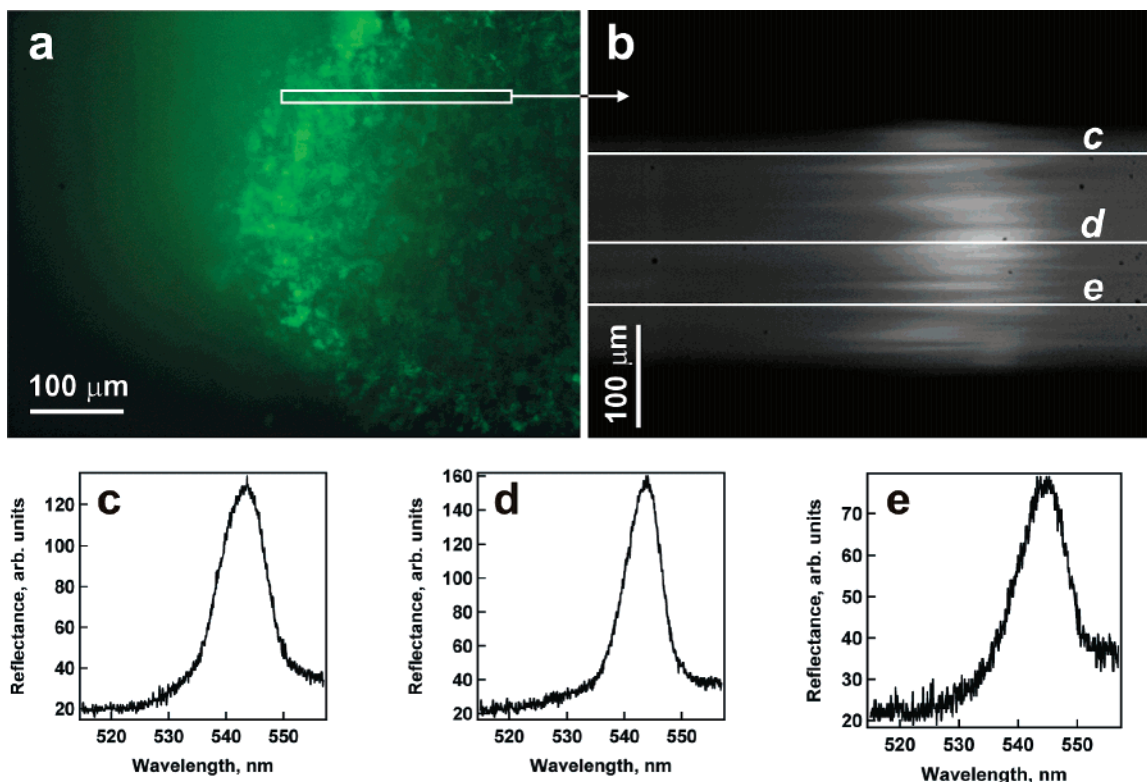


Figure 10. (a) Optical micrograph of the written crystalline phase following photothermal excitation of a bulk glassy sample. (b) Spectral image acquired from the indicated region of the real-space image. Bright spots in the image are indicative of high reflectivity and hence indicate the position and breadth of the Bragg peaks. (c–e) Line profiles taken from the indicated spots on the spectral image shown in b.

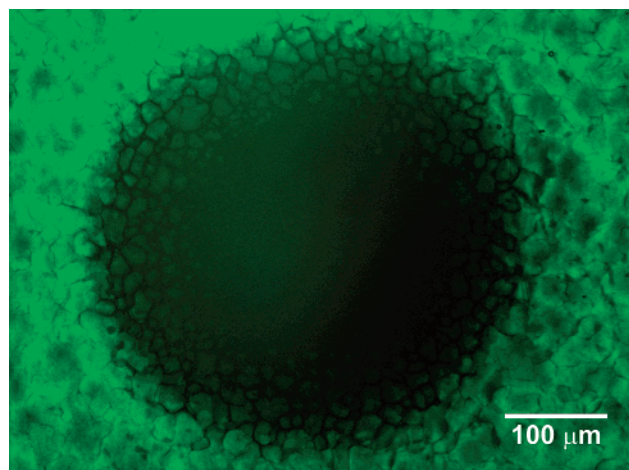


Figure 11. Optical micrograph of a glassy region photothermally introduced into a bulk crystalline sample containing 7.3×10^{13} Au particles/mL after 22 s of illumination at 3.4 W/cm^2 . Reproduced with permission from *J. Am. Chem. Soc.* **2003**, 125, 460–465. Copyright 2003 American Chemical Society.

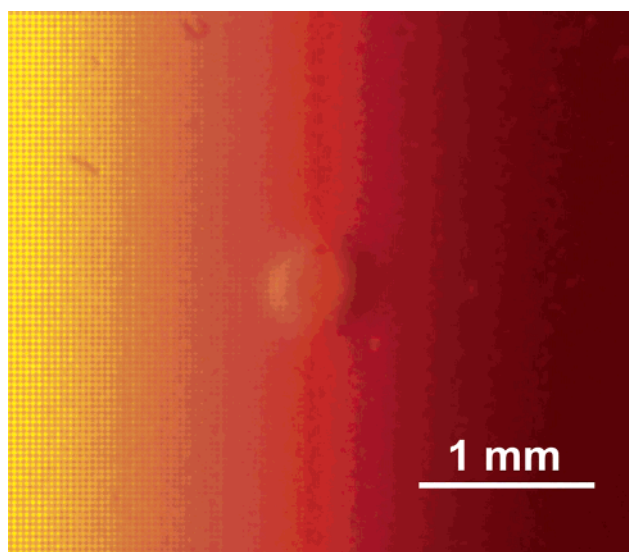


Figure 12. Photograph of an irradiated sample showing that the patterned region has a 3D structure and is hemispherical in shape. A diffuse backlight was used to adjust the contrast of the structure, which appears red because of the presence of colloidal Au. Reproduced with permission from *J. Am. Chem. Soc.* **2003**, 125, 5292–5293. Copyright 2003 American Chemical Society.

within the laser spot to control assembly. A well-defined Gaussian beam should induce a Gaussian-like profile of effective temperatures within the irradiated region. Thus, there should be a radial distribution of thermal crystallization conditions within the laser spot, which may give rise to different crystal morphologies and/or structures. We have found that by controlling the incident laser power one can use this effect to form a simple microlens inside of microgel colloidal crystal assemblies via photothermal patterning.^{37,38} A working microlens is possible because of a radially varying refractive index in the photothermally patterned region after laser irradiation, where the differing refractive indices are observable as a radial distribution of crystal lattice constants. A photograph of a representative composite material after 40 min of laser irradiation at 21°C is shown in Figure 12 and illustrates the apparent lens structure of the irradiated region. This photograph was taken of the sample on the opposite side from which laser irradiation was performed. The structure appears curved and seems to project out toward

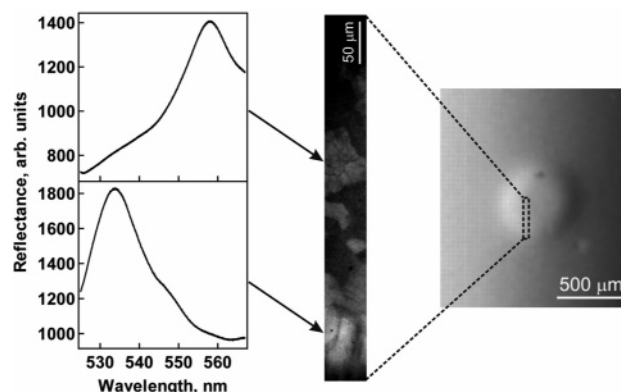


Figure 13. Microspectrophotometric analysis of the microlens shows a red shift in the Bragg peak from the periphery toward the inside. This change in lattice constant indicates that the refractive index changes radially within the irradiated region. Reproduced with permission from *J. Am. Chem. Soc.* **2003**, 125, 5292–5293. Copyright 2003 American Chemical Society.

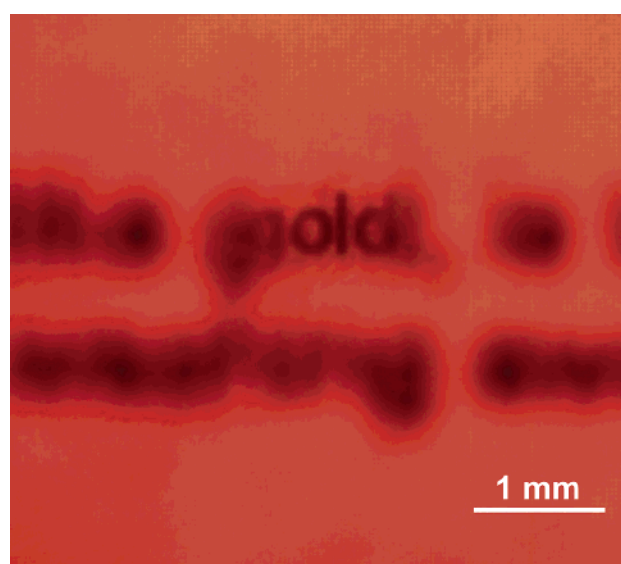


Figure 14. Two lines of text as seen through a microlens illustrating the focusing ability. The lens is located over the word “gold”, which is the only word within the two lines that is legible. The text on white paper is located 1.7 cm behind the sample. Reproduced with permission from *J. Am. Chem. Soc.* **2003**, 125, 5292–5293. Copyright 2003 American Chemical Society.

the viewer from the plane of the image. The red color in the image results from the presence of a Au colloid.

Although the lens shown in Figure 12 appears to be curved, this optical effect can be similarly produced by a planar structure with a radially varying *gradient* in refractive indices of the involved media. Indeed, an inspection of the optical properties of the irradiated region via microspectrophotometry (Figure 13) illustrates that the irradiated region acts as a gradient index structure, with spatially varying lattice constants and hence refractive indices. Toward the periphery of the irradiated region, the Bragg peak is at $\sim 535 \text{ nm}$. However, a red shift in the Bragg reflectance peak to $\sim 560 \text{ nm}$ occurs as the region toward the microlens interior is interrogated. A shift to a longer wavelength corresponds to an increase in the lattice constant for the hydrogel assembly. The particles are at a greater distance from one another near the center of the microlens region relative to particles near the periphery, suggesting that the individual microgels near the center are more hydrated than those near the periphery.³⁴ Differing degrees of particle hydration and concentration thus provide the refractive index difference

required for a working lens. The overall refractive index of the crystalline region is also apparently different from the surrounding overpacked glassy region, thus allowing lensing to occur.

The true hallmark of a working lens is illustrated in Figure 14, which shows the focusing ability of the microlens. In this case, the laser-incident side of the sample is closest to the photographic source. Two lines of black text on white paper were placed behind the sample, and the irradiated region was positioned over the word "gold" in the top line. The position of the text was varied behind the sample until focusing was achieved. It should be noted that these structures, although robust and long-lived enough to produce the data shown here, are metastable and transient in nature. The photothermally produced gradient in the lattice constant is stable over many hours but eventually homogenizes to a patterned region with a spatially invariant lattice constant. Obviously, this structure (such as that shown in Figure 9) displays no detectable lensing properties.

Summary

The results discussed above represent the initial stages of our work on soft colloidal assemblies. In these studies, we have discovered that the simple thermoresponsivity of the component particles enables broad and rapid control over the assembly and disassembly of the structures by small temperature excursions. This method can be used to tune the crystal lattice constant and thus modulate the Bragg reflections. We are continuing to investigate the fundamental issues associated with these assembly processes vis-à-vis the crystallization kinetics and the propagation of defects in these structures. It has also been observed that multiple weak attractive interactions such as hydrogen bonding can strongly perturb the phase behavior of these assemblies. In this case, the ability of the loosely cross-linked exterior of the particles to expand to maximize particle-particle contact enforces the crystalline phase at very low polymer concentrations. Continuing investigations are aimed at obtaining a deeper understanding of the crystallization thermodynamics and kinetics in soft associating systems. Finally, we presented our recent efforts in photopatterning of colloidal crystals by photothermal effects. The co-assembly of temperature-jump chromophores, such as Au nanoparticles, with microgels allows for facile patterning of photonic (crystalline) and nonphotonic (glassy) regions using laser illumination. Careful control of the incident power can also enable the writing of transient gradient index lens structures. We are currently focusing on improving the minimum line width attainable via this method as well as investigating the factors controlling image fidelity and stability. Beyond these studies, a huge range of opportunities exist in these materials, including those that take advantage of core/shell syntheses for surface or core-specific functionalization or methods for creating inorganic/organic hybrid structures displaying high refractive index contrast.

Acknowledgment. Various aspects of this work have been supported by the NSF (CHE-9984012), a Beckman Young Investigator Award to L.A.L., a Camille Dreyfus Teacher-Scholar Award to L.A.L., and the Office of Naval Research (N00014-03-1-0225).

References and Notes

- Alfrey, T., Jr.; Bradford, E. B.; Vanderhoff, J. W.; Oster, G. J. *Opt. Soc. Am.* **1954**, *44*, 603–609.
- Luck, W.; Klier, M.; Wesslau, H. *Ber. Bunsen-Ges.* **1963**, *67*, 75–83.
- Jones, J. B.; Sanders, J. V.; Segnit, E. R. *Nature* **1964**, *204*, 990–991.
- Sanders, J. V. *Nature* **1964**, *204*, 1151–1153.
- Sanders, J. V. *Acta Crystallogr., Sect. A* **1968**, *24*, 427–434.
- Iler, R. K. *Nature* **1965**, *207*, 472–473.
- Darragh, P. J.; Gaskin, A. J.; Terrell, B. C.; Sanders, J. V. *Nature* **1966**, *209*, 13–16.
- Greer, R. T. *Nature* **1969**, *224*, 1199–1200.
- Sanders, J. V.; Darragh, P. J. *Mineral. Rec.* **1971**, *2*, 261–268.
- Sanders, J. V.; Murray, M. J. *Nature* **1978**, *275*, 201–203.
- Murray, M. J.; Sanders, J. V. *Philos. Mag. A* **1980**, *42*, 721–740.
- Sanders, J. V. *Philos. Mag. A* **1980**, *42*, 705–720.
- Sanders, J. V. *J. Phys., Colloq.* **1985**, 1–8.
- vanBlaaderen, A.; Wiltzius, P. *Adv. Mater.* **1997**, *9*, 833–835.
- vanBlaaderen, A.; Ruel, R.; Wiltzius, P. *Nature* **1997**, *385*, 321–324.
- Murray, C. A.; Grier, D. G. *Annu. Rev. Phys. Chem.* **1996**, *47*, 421–462.
- Larsen, A. E.; Grier, D. G. *Nature* **1997**, *385*, 230–233.
- Gasser, U.; Weeks, E. R.; Schofield, A.; Pusey, P. N.; Weitz, D. A., *Science* **2001**, *292*, 258–262.
- Lin, K.-h.; Crocker, J. C.; Prasad, V.; Schofield, A.; Weitz, D. A.; Lubensky, T. C.; Yodh, A. G. *Phys. Rev. Lett.* **2000**, *85*, 1770–1773.
- Joannopoulos, J. D.; Meade, R. D.; Winn, J. N. *Photonic Crystals: Molding the Flow of Light*; Princeton University Press: Princeton, NJ, 1995.
- Thijssen, M. S.; Sprik, R.; Wijnhoven, J.; Megens, M.; Narayanan, T.; Lagendijk, A.; Vos, W. L. *Phys. Rev. Lett.* **1999**, *83*, 2730–2733.
- Blanco, A.; Chomski, E.; Grubbs, S.; Ibbett, M.; John, S.; Leonard, S. W.; Lopez, C.; Meseguer, F.; Miguez, H.; Mondia, J. P.; Ozin, G. A.; Toader, O.; van Driel, H. M. *Nature* **2000**, *405*, 437–440.
- Garcia-Santamaria, F.; Lopez, C.; Meseguer, F.; Lopez-Tejeda, F.; Sanchez-Dehesa, J.; Miyazaki, H. T. *Appl. Phys. Lett.* **2001**, *79*, 2309–2311.
- Vlasov, Y. A.; Bo, X.-Z.; Sturm, J. C.; Norris, D. J. *Nature* **2001**, *414*, 289–293.
- Yablonovitch, E.; Gmitter, T. J. *Phys. Rev. Lett.* **1989**, *63*, 1950–1953.
- John, S.; Wang, J. *Phys. Rev. Lett.* **1990**, *64*, 2418–2421.
- Yablonovitch, E.; Gmitter, T. J. *J. Opt. Soc. Am. A* **1990**, *7*, 1792–1800.
- Imhof, A.; Vos, W. L.; Sprik, R.; Lagendijk, A. *Phys. Rev. Lett.* **1999**, *83*, 2942–2945.
- Prasad, T.; Colvin, V.; Mittleman, D. *Phys. Rev. B* **2003**, *67*, 1–7.
- Kosaka, H.; Kawashima, T.; Tomita, A.; Notomi, M.; Tamamura, T.; Sato, T.; Kawakami, S. *Phys. Rev. B* **1998**, *58*, 10096–10099.
- Ochiai, T.; Sanchez-Dehesa, J. *Phys. Rev. B* **2001**, *64*, 245111–245117.
- Panoiu, N. C.; Bahl, M.; Osgood, R. M. *Opt. Lett.* **2003**, *28*, 2503–2505.
- Yu, X. F.; Fan, S. H. *Appl. Phys. Lett.* **2003**, *83*, 3251–3253.
- Debord, J. D.; Eustis, S.; Debord, S. B.; Lofey, M. T.; Lyon, L. A. *Adv. Mater.* **2002**, *14*, 658–661.
- Debord, J. D.; Lyon, L. A. *J. Phys. Chem. B* **2000**, *104*, 6327–6331.
- Debord, S. B.; Lyon, L. A. *J. Phys. Chem. B* **2003**, *107*, 2927–2932.
- Jones, C. D.; Serpe, M. J.; Schroeder, L.; Lyon, L. A. *J. Am. Chem. Soc.* **2003**, *125*, 5292–5293.
- Jones, C. D.; Lyon, L. A. *J. Am. Chem. Soc.* **2003**, *125*, 460–465.
- Pieranski, P. *Contemp. Phys.* **1983**, *24*, 25–73.
- Pusey, P. N.; van Megan, W. *Nature* **1986**, *330*, 340–342.
- Aste, T.; Weaire, D. *The Pursuit of Perfect Packing*; Institute of Physics: Bristol, England, 2000.
- Kepler, J. *The Six-Cornered Snowflake*; Clarendon Press: Oxford, England, 1966.
- Holden, C. *Science* **2003**, *299*, 1512.
- Zong, C.; Talbot, J. *Sphere Packings*; Springer-Verlag: New York, 1999.
- Szpiro, G. *Nature* **2003**, *424*, 12–13.
- See <http://www.math.pitt.edu/~thales/> for details of the proof.
- Lee, W.; Pruzinsky, S. A.; Braun, P. V. *Adv. Mater.* **2002**, *14*, 271–274.
- Ackerson, B. J.; Paulin, S. E.; Johnson, B.; van Megen, W.; Underwood, S. *Phys. Rev. E* **1999**, *59*, 6903–6913.
- Jiang, P.; Bertone, J. F.; Hwang, K. S.; Colvin, V. L. *Chem. Mater.* **1999**, *11*, 2132–2140.
- Holland, B. T.; Blanford, C. F.; Do, T.; Stein, A. *Chem. Mater.* **1999**, *11*, 795–805.
- Holland, B. T.; Blanford, C.; Stein, A. *Science* **1998**, *281*, 538–540.
- Torquato, S.; Truskett, T. M.; Debenedetti, P. G. *Phys. Rev. Lett.* **2000**, *84*, 2064–2067.
- Truskett, T. M.; Torquato, S.; Debenedetti, P. G. *Phys. Rev. E: Stat. Phys., Plasmas, Fluids, Relat. Interdiscip. Top.* **2000**, *62*, 993–1001.
- Vanblaaderen, A.; Wiltzius, P. *Science* **1995**, *270*, 1177–1179.

- (55) Kesavamoorthy, R.; Arora, A. K. *J. Phys. C: Solid State Phys.* **1986**, *19*, 2833–2846.
- (56) Weeks, E. R.; Weitz, D. A. *Chem. Phys.* **2002**, *284*, 361–367.
- (57) Dinsmore, A. D.; Weitz, D. A. *J. Phys.: Condens. Matter* **2002**, *14*, 7581–7597.
- (58) Weeks, E. R.; Weitz, D. A. *Phys. Rev. Lett.* **2002**, *89*, 1–4.
- (59) Rintoul, M. D.; Torquato, S. *Phys. Rev. E: Stat. Phys., Plasmas, Fluids, Relat. Interdiscip. Top.* **1998**, *58*, 532–537.
- (60) Peltou, R. *Adv. Colloid Interface Sci.* **2000**, *85*, 1–33.
- (61) Murray, M. J.; Snowden, M. J. *Adv. Colloid Interface Sci.* **1995**, *54*, 73–91.
- (62) Saunders, B. R.; Vincent, B. *Adv. Colloid Interface Sci.* **1999**, *80*, 1–25.
- (63) Xu, S.; Zhang, J.; Paquet, C.; Lin, Y.; Kumacheva, E. *Adv. Funct. Mater.* **2003**, *13*, 468–472.
- (64) Pham, H. H.; Kumacheva, E. *Macromol. Symp.* **2003**, 192(7th Pacific Polymer Conference, 2001), 191–205.
- (65) Weissman, J. M.; Sunkara, H. B.; Tse, A. S.; Asher, S. A. *Science* **1996**, *274*, 959–960.
- (66) Hellweg, T.; Kratz, K.; Pouget, S.; Eimer, W. *Colloids Surf., A* **2002**, *202*, 223–232.
- (67) Hellweg, T.; Dewhurst, C. D.; Bruckner, E.; Kratz, K.; Eimer, W. *Colloid Polym. Sci.* **2000**, *278*, 972–978.
- (68) Senff, H.; Richtering, W. *J. Chem. Phys.* **1999**, *111*, 1705–1711.
- (69) Gao, J.; Hu, Z. *Langmuir* **2002**, *18*, 1360–1367.
- (70) Hu, Z.; Lu, X.; Gao, J. *Adv. Mater.* **2001**, *13*, 1708–1712.
- (71) Reese, C. E.; Mikhonin, A. V.; Kamenjicki, M.; Tikhonov, A.; Asher, S. A. *J. Am. Chem. Soc.* **2004**, *126*, 1493–1496.
- (72) Heskins, M.; Guillet, J. E. *J. Macromol. Sci., Chem.* **1968**, *A2*, 1441–1455.
- (73) Wu, C.; Wang, X. *Phys. Rev. Lett.* **1998**, *80*, 4092–4094.
- (74) Wu, C.; Zhou, S.; Au-Yeung, S. C. F.; Jiang, S. *Angew. Makromol. Chem.* **1996**, *240*, 123–136.
- (75) Wu, C.; Zhou, S. *J. Macromol. Sci., Phys.* **1997**, *B36*, 345–355.
- (76) Wu, C. *Polymer* **1998**, *39*, 4609–4619.
- (77) Shibayama, M.; Tanaka, T. Volume Phase Transition and Related Phenomena of Polymer Gels. In *Advances in Polymer Science*; Springer-Verlag: Berlin, 1993; Vol. 109, pp 1–62.
- (78) Debord, J. D.; Lyon, L. A. *Langmuir* **2003**, *19*, 7662–7664.
- (79) Senff, H.; Richtering, W. *Colloid Polym. Sci.* **2000**, *278*, 830–840.
- (80) Crowther, H. M.; Vincent, B. *Colloid Polym. Sci.* **1998**, *276*, 46–51.
- (81) Pan, G. S.; Kesavamoorthy, R.; Asher, S. A. *Phys. Rev. Lett.* **1997**, *78*, 3860–3863.
- (82) Pan, G. S.; Kesavamoorthy, R.; Asher, S. A. *J. Am. Chem. Soc.* **1998**, *120*, 6525–6530.
- (83) Foulger, S. H.; Kotha, S.; Sweryda-Krawiec, B.; Baughman, T. W.; Ballato, J. M.; Jiang, P.; Smith, D. W., Jr. *Opt. Lett.* **2000**, *25*, 1300–1302.
- (84) Foulger, S. H.; Jiang, P.; Lattam, A. C.; Smith, D. W., Jr.; Ballato, J. *Langmuir* **2001**, *17*, 6023–6026.
- (85) Figotin, A.; Godin, Y. A.; Vitebsky, I. *Phys. Rev. B: Condens. Matter* **1998**, *57*, 2841–2848.
- (86) Urbas, A.; Sharp, R.; Fink, Y.; Thomas, E. L.; Xenidou, M.; Fetters, L. J. *Adv. Mater.* **2000**, *12*, 812–814.
- (87) Jones, C. D.; Lyon, L. A. *Langmuir* **2003**, *19*, 4544–4547.
- (88) Jones, C. D.; Lyon, L. A. *Macromolecules* **2003**, *36*, 1988–1993.
- (89) Gan, D.; Lyon, L. A. *Anal. Chim. Acta* **2003**, *496*, 53–63.
- (90) Gan, D.; Lyon, L. A. *Macromolecules* **2002**, *35*, 9634–9639.
- (91) Wang, J.; Gan, D.; Lyon, L. A.; El-Sayed, M. A. *J. Am. Chem. Soc.* **2001**, *123*, 11284–11289.
- (92) Gan, D.; Lyon, L. A. *J. Am. Chem. Soc.* **2001**, *123*, 8203–8209.
- (93) Gan, D.; Lyon, L. A. *J. Am. Chem. Soc.* **2001**, *123*, 7511–7517.
- (94) Jones, C. D.; Lyon, L. A. *Macromolecules* **2000**, *33*, 8301–8306.
- (95) Wu, C.; Zhou, S. *Macromolecules* **1997**, *30*, 574–576.
- (96) Grier, D. G. *J. Phys.: Condens. Matter* **2000**, *12*, A85–A94.
- (97) Gilanyi, T.; Varga, I.; Meszaros, R.; Filipcsei, G.; Zrinyi, M. *Phys. Chem. Chem. Phys.* **2000**, *2*, 1973–1977.
- (98) Varga, I.; Gilanyi, T.; Meszaros, R.; Filipcsei, G.; Zrinyi, M. *J. Phys. Chem. B* **2001**, *105*, 9071–9076.
- (99) Link, S.; El-Sayed, M. A. *Int. Rev. Phys. Chem.* **2000**, *19*, 409–453.
- (100) Vlasov, Y. A.; Deutsch, M.; Norris, D. J. *Appl. Phys. Lett.* **2000**, *76*, 1627–1629.